Electronic Supplementary Material (ESI) for RSC Advances.

Entrapment and Characterization of Functional Allosteric Conformers of Hemocyanin in Sol-Gel Matrices.

Fabrizio Minute[a], Nadja Hellmann[b], Francesco Spinozzi[c], Maria Grazia Ortore[c], Paolo Di Muro[a], Luigi Bubacco[a] and Mariano Beltramini[a]*

[a] Department of Biology, University of Padova, Via Ugo Bassi 58B, I-35131 Padova, Italy

[b] Institute for Molecular Biophysics, University of Mainz, Jakob-Welder-Weg, Mainz, Germany

[c] Department DISVA, Marche Polytechnic University and CNISM, Via Brecce Bianche, I-60131 Ancona, Italy

SUPPLEMENTARY INFORMATION

S1 Sample holders

Spectroscopic experiments involving silica sol-gel matrix required the development of suitable cells and sample holders. To this aim we designed and constructed specific Teflon cells with optical windows (Fig. S1 *A*). The dimension of the cells are 9 mm (*width*) x 32 mm (*height*) x 3 mm (*thickness*), allowing the inclusion into quartz cuvettes with a standard commercial size. Internal optical window with a width of 3 mm was designed taking account of the beam size of the spectroscopic techniques applied in this work. We also designed a sample holder for X-ray absorption spectroscopy (XAS). It consists of two blocks of Teflon (a single block is shown in Fig. S1 *B*) with a hollow central rectangular area (9 mm x 32 mm x 1.5 mm). When the two blocks are combined together they define an internal cavity, having the same size and dimension as the Teflon cell. Therefore the Teflon cell with the polymerized gel perfectly fits into this pocket. The two optical windows of the sample holder can be covered with Kapton films and the optical window space between the internal Teflon cell and the external surface of the sample holder can be filled with buffer, through the two holes at the top of the holder (Fig. S1 *C*).

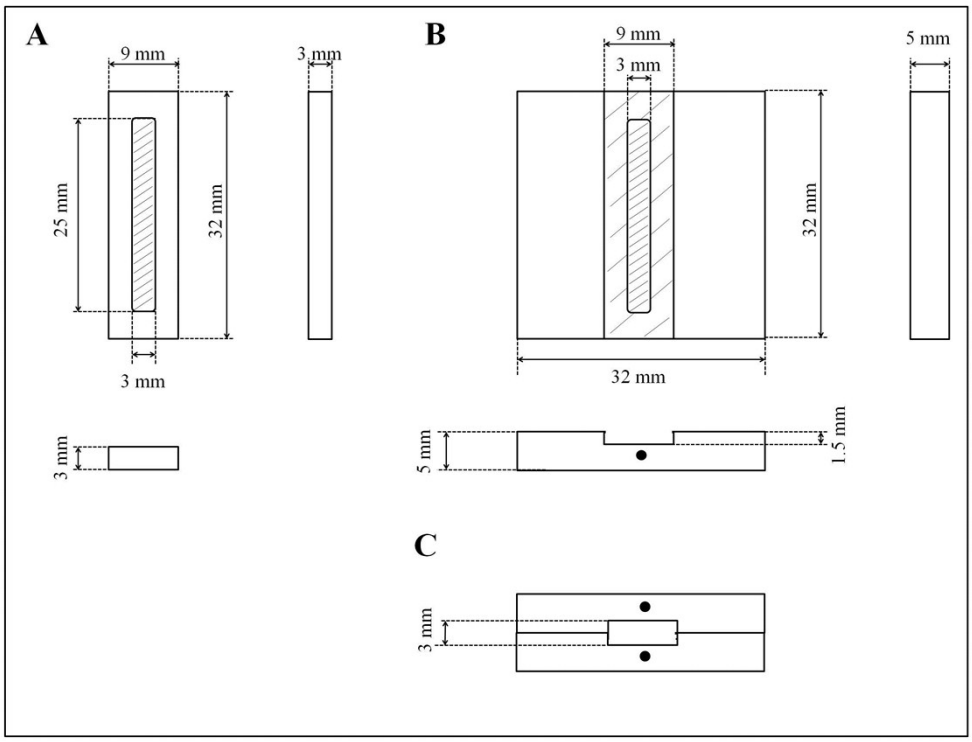

Fig. S1: Details of the Teflon cell and sample holder designed for spectroscopic experiments. Top, front and side views of the Teflon cell (*A*) and "half" sample holder are reported (*B*). Only top view of the "full" sample holder is shown (*C)*, with the two holes indicated as black circles.

S2 Measurements of Small Angle X-rays Scattering (SAXS) to characterize the sol-gel porosity

SAXS measurements have been performed at room temperature at the Elettra Synchrotron Radiation facility (Trieste, Italy) and were used to characterize the properties of the orthosilicate matrix as a function of the different experimental conditions used for oxygen binding experiments. The wavelength of the incident X-ray beam was λ =1.54 Å (at E = 8 keV) and the explored Q-range extended from 0.019 to 0.46 $Å^{-1}$, where $Q = 4\pi \sin\theta/\lambda$ and 2θ is the scattering angle. The *Mar300 Image Plate* with a circular active area of 180 mm in diameter and with a spatial resolution (pixel size) of 150 µm was used, and the sample-detector distance was set to 1.78 m. Undoped sol-gel samples were measured into quartz capillaries (diameter 1 and 1.5 mm, wall thickness 0.01 mm), mounted on an aluminum sample holder with a circular cutout. The recorded 2D scattering patterns (1200x1200 pixels) were converted using the *Fit2D* program. Data reduction, involving flux, exposure time and sample transmission normalization, was performed using in-house programs. SAXS spectra were analyzed using the *GENFIT* program[59], through the application of a mass fractal model [58]. This model describes the sol-gel matrix in terms of a porous network formed

by the aggregation of spherical silica particles of radius r_0. In particular, the ordering of the spherical primary particles within the cluster can be described by the following interparticle structure factor *S(Q)*:

$$S(Q) = 1 + \frac{\sin\left[(D_f - 1)\tan^{-1}(Q\xi)\right]}{(Qr_0)^{D_f}} \frac{D_f \Gamma(D_f - 1)}{\left[1 + 1/(Q^2\xi^2)\right]^{(D_f - 1)/2}} \qquad \text{Eq. S1}$$

where D_f is the fractal dimension, Γ the gamma function and ξ is the cutoff distance of the fractal correlation, which can be interpreted as the pore size in the gels[64].

The parameters of all the experiments are summarized in Table S1. From these results it appears that the fractal dimension D_f is not affected by changes of pH, aging time or glycerol content (average value 2.5±0.3), whereas the radius r_0 decreases in presence of 25% glycerol (Table S1 and Fig. S2). The box-plots confirm the effect of glycerol on the radius r_0, with a significantly decrease of the average value from 10±2Å in absence of glycerol to 6±2Å in presence of 25% glycerol. On the contrary, pH and aging do not affect this parameter. More complicated is the analysis of the cutoff distance ξ due to the high variability of this parameter. In fact, the presence of two very high values (380±50 Å and 330±80 Å), identified as outliers, makes it difficult to estimate the effects of the three experimental conditions. The average value of ξ is 140±100Å, considering all the values, and 90±20Å without outliers. Considering that the hemocyanin investigated in this work is a dodecamer made up of two hexamers of ~90 Å, the best condition would be represented by a matrix with pores size of ~200 Å. Indeed, under the experimental conditions of spectroscopic and SANS characterization (pH 7.8, 25% glycerol, 2 days aging) the size of sol-gel pores (330±80 Å) is comparable to that of hemocyanin dodecamers.

The lower dimensions of the silica particles in presence of 25% of glycerol come along with better UV/visible absorption spectra of the sol-gel matrix prepared at this condition, compared to the one prepared in absence of glycerol (Fig. S3). Indeed, as reported by Rabinovich[65], the optical properties of the sol-gel matrix depend on the size of the colloidal particles that aggregate forming the gel. The transparence of the matrix was also confirmed by the CD and fluorescence emission spectra (not shown), although in the latter case the spectra were slightly affected by light scattering. We therefore used the glycerol containing orthosilicate throughout at the desired pH and aging time as necessary for the sample preparations. These two factors did not influence the sol-gel optical properties, at least within the range of conditions explored in this work. The

increase of the fractal dimension in function of the aging time described by Nair et al.[66] could not be confirmed in this work.

Glycerol (%)	**pH**	**Aging (days)**	D_f	r_0 **(Å)**	r_0 **dispersion (%)**	ξ **(Å)**
0	*6.5*	*2*	2.32±0.02	11.9±0.6	30±1	89±5
0	*6.5*	*6*	2.35±0.02	11.5±0.6	20±1	76±4
0	*7.5*	*2*	2.45±0.01	6.8±0.4	36±1	89±2
0	*7.5*	*6*	2.86±0.02	9±1	25±1	83±4
0	*7.8*	*2*	2.78±0.02	10.4±0.6	21±1	81±2
0	*7.8*	*6*	2.04±0.01	10.7±0.2	32±1	120±10
25%	*6.5*	*2*	2.93±0.01	6.3±0.5	22±1	97±3
25%	*6.5*	*6*	2.36±0.01	8.3±0.2	20±1	380±50
25%	*7.5*	*2*	2.61±0.01	5.0±0.1	21±1	69±1
25%	*7.5*	*6*	2.22±0.01	5.0±0.1	22±1	69±1
25%	*7.8*	*2*	1.93±0.01	5.1±0.1	41±1	330±80
25%	*7.8*	*6*	2.83±0.01	8.1±0.6	25±1	150±10

Tab. S1. Characteristics of silica sol-gel matrix at different conditions *(% of glycerol, pH and aging*) calculated from SAXS spectra. D_f is the fractal dimension; r_0 the radius of the spherical particles; r_0 dispersion (*%*) is the dispersion of the radius expressed in percentage; ξ is the cutoff distance. Buffer: 50 mM Tris/HCl, 20 mM $CaCl_2$, glycerol and pH as indicated. Average values and standard deviations of the parameters are calculated by repeating for fifty times the analysis of SAXS curves. For each repetition, the experimental SAXS data are randomly moved within their error bar.

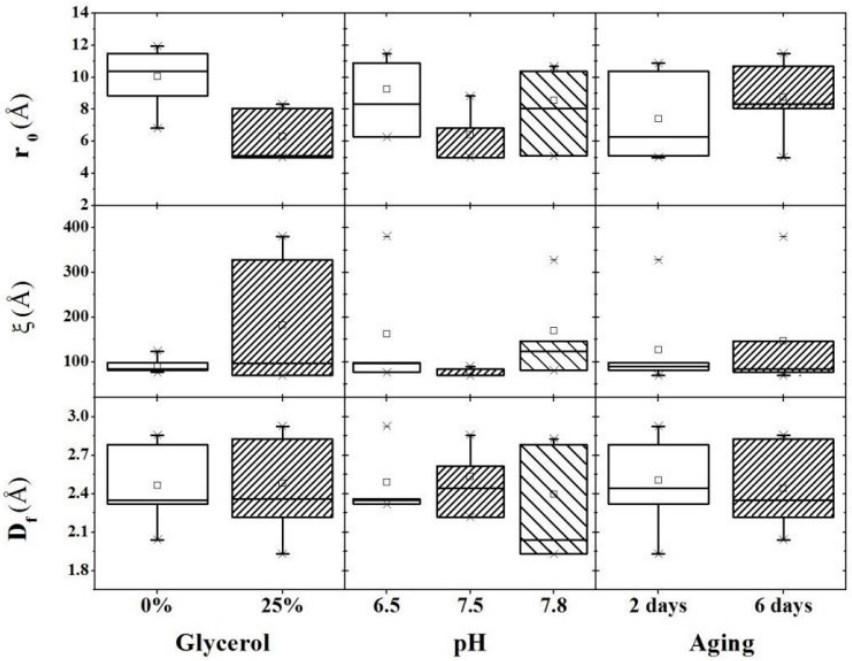

Fig. S2: Box-plot representation of the radius of the spherical particles r_0, the correlation length ξ and the fractal dimension D_f of the silica matrix in presence/absence of 25% glycerol (*first column*), at pH 6.5, 7.5 and 7.8 (*second column*) and after 2 and 6 days of aging (*third column*). Buffer: 50 mM Tris/HCl, 20 mM $CaCl_2$, glycerol and pH as indicated.

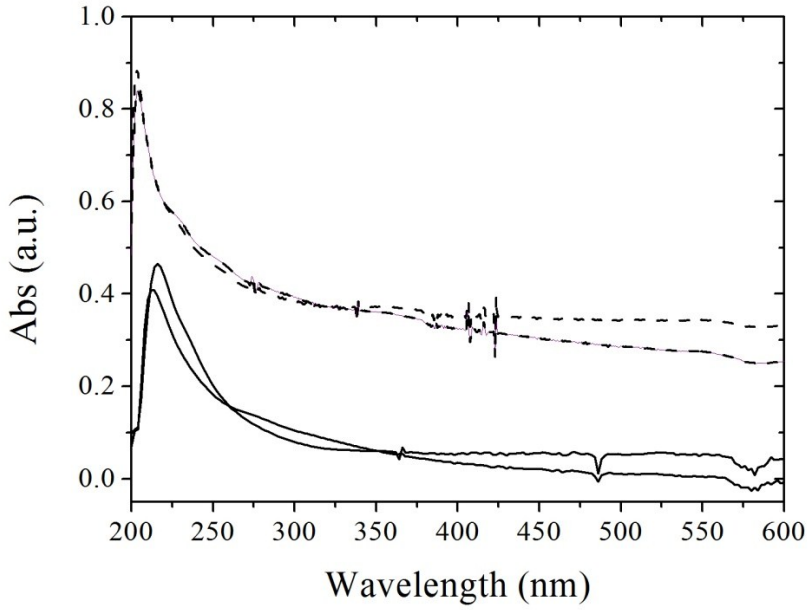

Fig. S3: UV-visible absorption spectra of sol-gel matrix prepared in the presence of 25% glycerol (*solid line***)** and absence of glycerol (*dashed lines*). Spectra of two different preparations for each condition are presented. Buffer: Buffer: 50 mM Tris/HCl, 20 mM $CaCl_2$, pH 7.8.

S3 Measurements of Small Angle Neutron Scattering (SANS) to characterize the quaternary structure of embedded hemocyanin

For SANS measurements, sol-gels with and without entrapped hemocyanin (5 g L^{-1}) were prepared at pH 7.8 in H_2O and polymerized into 1- and 2-mm path length quartz cuvettes with two open ends (total length of cuvette 4.5 mm). Once the gel is formed inside, the cuvettes were incubated for 24 h in rinse solutions containing different amount of D_2O and H_2O to ensure efficient hydrogen–deuterium exchange. The rinse solutions at the selected degree of deuteration x_D (x_D=2[D_2O]/{2[D_2O]+2[H_2O]+[H_{exg}]}, where [H_{exg}] represents the molar concentration of the exchangeable protons arising from all the molecules in the sample, excluding the light water) were prepared by diluting a mother solution at pH 7.4 with 25% v/v glycerol. The composition of the mother solution and the rinse solutions are reported in Table S2 and S3 (see below). A pH value of 7.4 was calculated for samples prepared in D_2O based on the relationship pD = pH meter reading + 0.4[67]. SANS measurements were carried out at the ILL neutron radiation facility (Grenoble, France), on the instruments D11 and D22. Undoped sol-gel samples were recorded at D11 in a range of 0.009-0.175 $Å^{-1}$ for the scattering vector Q, ($Q=4\pi \sin\theta/\lambda$, 2θ being the scattering angle and λ the neutron wavelength). The standard contrast variation analysis, based on the evaluation of the root mean square of the scattered intensities (macroscopic differential cross sections, $d\Sigma/d\Omega(Q)$) extrapolated at Q=0 as a function of x_D), allows to determine the optimum value of x_D that eliminates the difference between the scattering length density of the silica gel and the one of the buffer (matching point).

The following compositions of the *mother solution* and the *rinse solutions* were used (Tab. S2, S3).

Concentration (Unit)	H_2O*	D_2O	Tris	HCl (37%)	$CaCl_2$	Na-Lactate **
M	0.540	53.874	0.162	0.157	0.065	0.130
g/L	9.722	1078.962	19.625	5.710	7.192	14.53
w/w	0.009	0.962	0.018	0.005	0.006	0.013
mol/mol	0.010	0.983	0.003	0.003	0.001	0.002
v/v	0.010	0.973	0.010	0.003	0.005	0.008

Tab. S2: Mother solution composition.
* H_2O derived from the 35% w/w HCl.
** Samples were prepared both in presence and absence of sodium lactate.

x_D	V total (µL)	V glycerol pure (µL)	V *mother solution* (µL)	V D_2O pure (µL)	V H_2O pure (µL)
0.60	9000	2487	2989	1582.4	2007.0
0.70	9000	2487	2989	2330.7	1258.7
0.72	9000	2487	2989	2480.4	1109.0
0.80	9000	2487	2989	3079.0	510.4
0.86	9000	2487	2989	3527.9	61.5

Tab. S3: Rinse solutions composition at different degrees of deuteration (x_D).

Our first aim was to find the optimum ratio D_2O/H_2O for the preparation of the samples, to remove the contribution of the silica matrix to the experimental scattering pattern. According to atomic scattering lengths, molecular volumes and exchangeable hydrogens of all the species and also considering the volume contraction that follows the polymerisation of the tetramethyl orthosilicate (TMOS), we had found the theoretical value of the deuteration degree (x_D=0.73) to achieve a perfect match between the scattering length density of the gel (in *orange*) and the one of the hydrating solution (in *blue*) (Fig. S4).

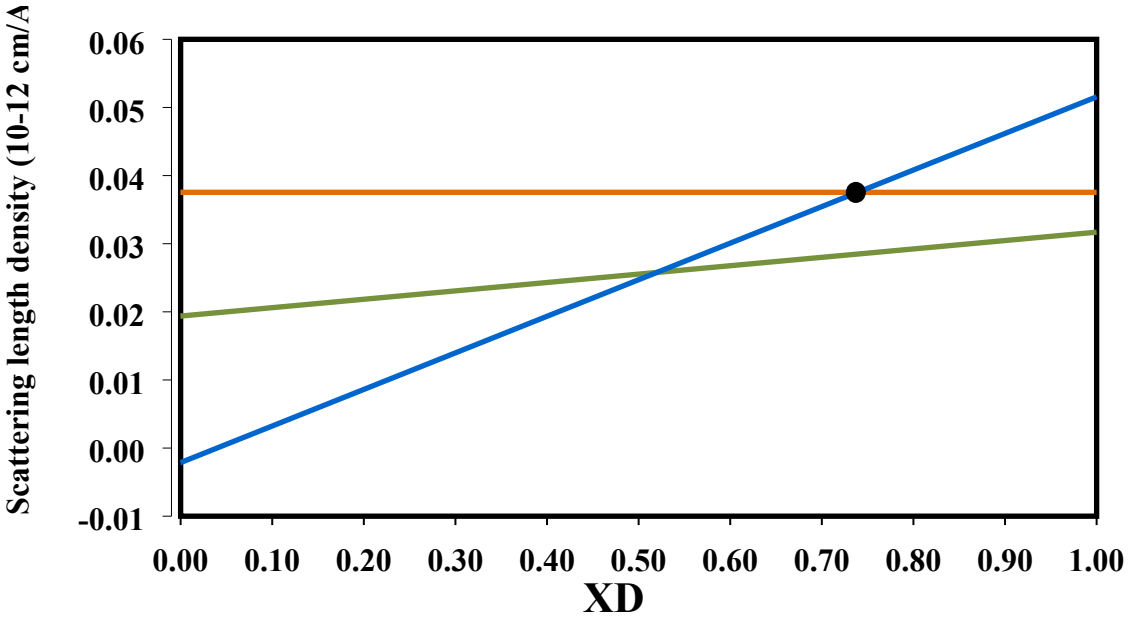

Fig. S4: Scattering length density of buffer (*in blue*), sol-gel matrix (*in orange*) and hemocyanin (*in blue*). The theoretical value of x_D at which silica matrix is perfectly matched is 0.73 (*black dot*).

The optimum x_D value was also experimentally determined by measuring sol-gel matrices without trapped hemocyanin at four different values for x_D: 0.6, 0.70, 0.80 and 0.86. Initially, samples were prepared directly at the specific x_D, but D_2O seemed to affect the gelification process of the matrix. Therefore, we decided to prepare samples in H_2O and, once the sol-gel polymerized, dialyzed them against the solutions at the four x_D. To permit the diffusion of the mother solution through the matrix, the gels were polymerized into quartz cuvette (1 mm and 2 mm thickness) with both ends open. SANS profiles exhibited by these gels are shown in Fig. S5 (*A-B*).

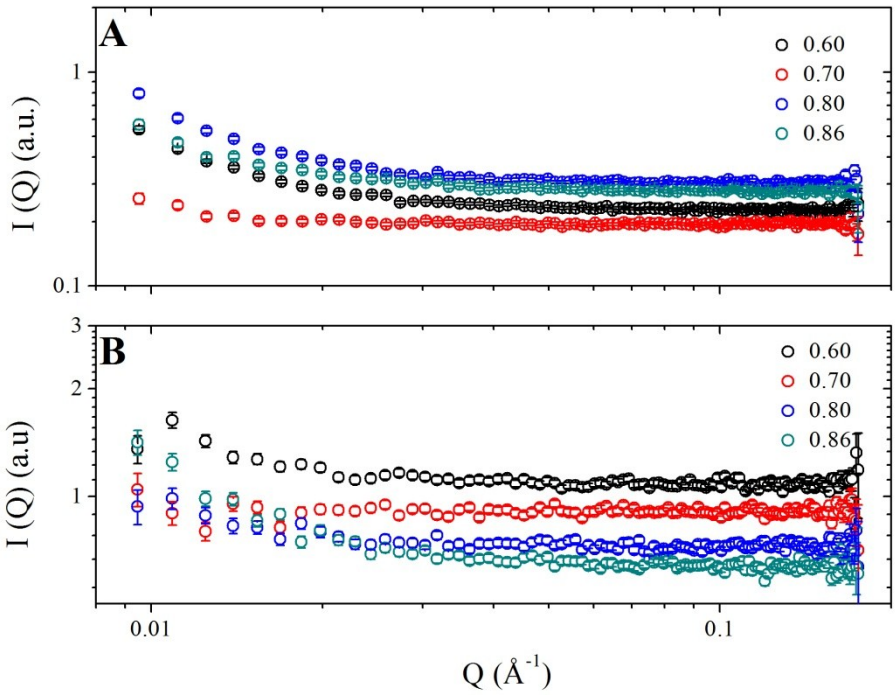

Fig. S5 Semilogarithmic SANS spectra of undoped sol-gel matrix at different x_D. The spectra of sol-gel matrices prepared in cuvette of either 1 mm or 2 mm thickness are reported in panel A and B, respectively. Samples at pH 7.8 and different x_D (0.6, 0.70, 0.80 and 0.86) as indicated (see Tab. S2 and S3).

The optimum x_D was calculated by plotting the square root of the scattering cross sections versus x_D and extrapolate to Q=0 (I(0)) for each SANS spectra. An expected, a linear trend as a function of x_D was observed (Fig. S6). The value for the sol-gel contrast match was x_D= 0.673 using cuvettes of 1 mm thickness and x_D=0.720 using cuvettes of 2 mm thickness. The better results in terms of linearity were obtained for samples with 2 mm thickness (R^2=0.99), probably because they allow a better exchange between gel and embedding solution.

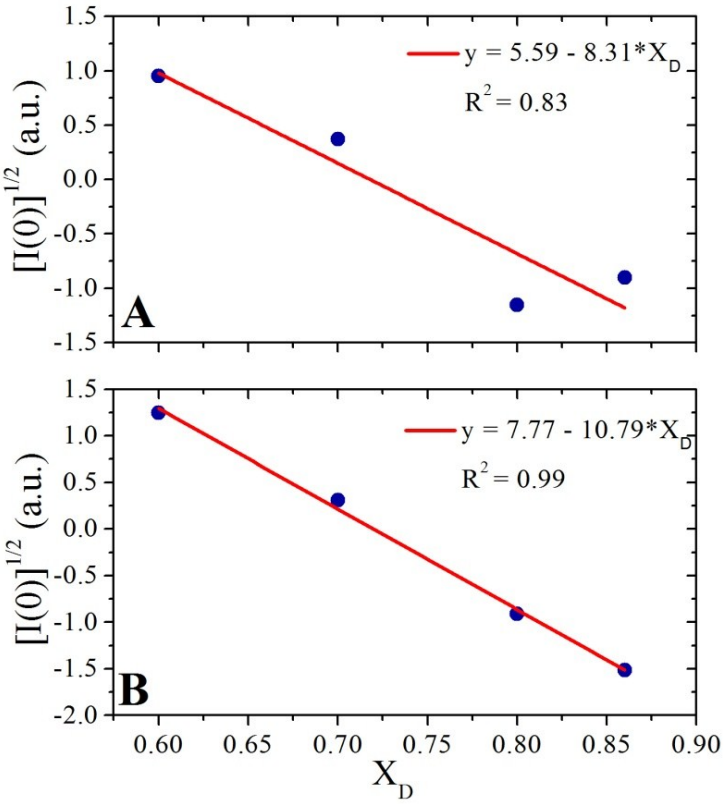

Fig. S6. Plot of $[I(0)]^{1/2}$ as a function of x_D (*A: 1mm cuvette thickness; B: 2mm cuvette thickness*). The linear fit of the four points is reported in red.

S4 Analysis of oxygen binding data

The data points for each condition were combined to one binding curve. Since not for all conditions sufficient data were collected to calculate mean and standard deviations for each oxygen concentration, all data points were used in the analysis, and no weighting was performed.

Identification of a suitable model and characterisation of the oxygen binding constants

To determine which cooperative model is suitable to describe the oxygen binding curves, first solution data only were considered. Different models were fitted in a global analysis taking into account all conditions (pH, ± L-lactate) (see eq. 3 and eq. 4). The resulting common binding constants are summarized in Tab. S4.

4 state	value ($Torr^{-1}$)	Nested MWC	value ($Torr^{-1}$)	3 state	value ($Torr^{-1}$)
K_W	0.0024	K_{tT}	0.0041	K_T	0.0021
K_T	0.0208	K_{tR}	0.0317	K_S	0.0366
K_S	0.0422	K_{rR}	0.3263		
K_R	0.6706	K_{rT}	0.7044	K_R	0.6028
SS^2	0.138		0.145		0.142
DF	188		188		194
$10^3*SS^2/DF$	0.734		0.771		0.732

Tab. S4. Results of global analysis of solution data: All solution data measured for the five different conditions (*pH 6.5 ± L-lactate, pH 7.5, pH 7.8 ± L-lactate*) were analyzed simultaneously based on the indicated models. Binding constants characteristic for each model were forced to be identical for all conditions, whereas an individual set of allosteric equilibrium constants were assigned to each condition. SS^2 indicates the squared residuals for each analysis, and DF the corresponding degrees of freedom. Errors for the binding constants were not delivered by the fitting routine, indicating a strong dependency on each other and on the exact value of the allosteric equilibrium constants.

The comparison of the three models employed shows that based on solution data alone one would not deduce a requirement for more than three conformations, based on SS^2/DF. The binding constant for the conformation with the lowest and highest affinity is similar for all three models. To check whether inclusion of data from embedded hemocyanin indicates the presence of four conformations, for each condition the corresponding three curves (solution, Oxy^{EM}, $Deoxy^{EM}$) were analyzed simultaneously. Since in a previous study[24] oxygen binding from this hemocyanin could successfully be described by the Nested-MWC-model, the following strategy was employed: first, the simplest linear model (two, three or four-state model) compatible with the data was determined. For comparison, the data were analyzed based on the Nested-MWC-model. If some conformations do not play any role for a particular condition, an analysis based on four conformations leads to results, where several binding constants have the same value or the routine does not converge. In these cases, the binding constants not contributing were identified by comparing the values for the binding constants determined for the linear models with less than four conformations with the binding constants for the Nested-MWC-model and set constant. For example at pH 6.5, only the conformations with the lowest affinities occur in significant amounts. Thus, in the analysis based on the Nested-MWC-model, k_{rT} and k_{rR} was set constant to the values

summarized in Tab. S4 for the corresponding model and marked grey (Tab. S5). At pH 7.5 two of the four binding constants are very similar, but a very low affinity conformation is missing; indicating that tT is not contributing much.

condition	pH 6.5	pH 6.5 + L	pH 7.5	pH 7.8		pH 7.8 + L
min. # conformations linear model	2	2	4	4		2
K_1,K_2,K_3,K_4 [Torr^{-1}]	0.0031/ 0.039	0.0031/ 0.246	0.012/ 0.052/ 0.064/ 0.382	0.043/ 0.158/ 0.475/ 2.3		0.085/ 1.15
10^3*SS²/DF	0.74	0.99	0.91	0.86		1.44
Nested-MWC-Model						
K_{tT} [Torr^{-1}]	0.0031±0.0006	0.004	0.004	0.004	0.004	0.004
K_{tR} [Torr^{-1}]	0.039±0.004	0.031±0.004	0.017± 0.008	0.043	0.036	0.0317
K_{rR} [Torr^{-1}]	0.3	0.19±0.11	0.083±0.092	0.158	0.135	0.13±0.02
K_{rT} [Torr^{-1}]	0.7	0.7	0.7	0.475	0.7	0.9±0.27
10^3* SS²/DF	0.49	0.99	0.91	0.91	0.97	1.61

Tab. S5. Results for the oxygen binding constants including sol-gel data: For each condition, the corresponding three sets of data *(solution, Oxy^{EM}, $Deoxy^{EM}$)* were analyzed simultaneously, yielding a common set of binding constants. The minimal number of conformations employing a linear model is indicated, together with the values for the corresponding binding constants (*K_1, K_2, K_3, K_4*). The results of employing the Nested-MWC-model are summarized in the lower part. Here, in all cases some of the binding constants tend to be the same if all four are let free for optimisation; thus, one or two were set constant to values as obtained from the global analysis of all solution data (*marked in grey*). SS² indicates the squared residuals for each analysis, and DF the corresponding degrees of freedom.

The results indicate that the Nested-MWC-model is a suitable model for the present set of data. To refine the corresponding oxygen binding constants, a second round with slightly altered values for those conformations set fixed in the routine was applied, with the aim to obtain more similar values for the oxygen binding constants under different conditions (Tab. S6).

	pH 6.5	pH 6.5+L	pH 7.5	pH 7.8	pH 7.8 + L
K_{tT} [Torr^{-1}]	0.0031±0.0004	0.003	0.003	0.003	0.003
K_{tR} [Torr^{-1}]	0.021±0.002	0.031±0.005	0.03± 0.01	0.036	0.03
K_{rR} [Torr^{-1}]	0.13	0.2±0.1	0.1±0.1	0.137	0.13±0.02
K_{rT} [Torr^{-1}]	0.9	0.9	0.9	0.9	0.9±0.1
10^3* SS²/DF	0.49	0.99	1.04	9.7	1.58

Tab. S6. Refined results for the oxygen binding constants including sol-gel data: The procedure is as described for Tab. S5. For all cases the value for the regression coefficient r^2 is > 0.991.

Determination of the allosteric equilibrium constants and conformational distributions

So far we obtained a set of oxygen binding constants describing the available set of data with a good agreement (r^2 > 0.991 for each condition). To determine the allosteric equilibrium constants characteristic for each condition, each data set was analyzed individually, with the binding constants set equal to the values given in Tab. S6. As mentioned above, in some cases not all conformations contribute to the binding curve; in these cases only limits or constraints can be given for some of the allosteric equilibrium constants (Tab. S7). Based on these values the corresponding conformational distribution at 0 Torr and 760 Torr was calculated and compared to the conformations arrested in the sol-gel, where applicable (Tab. S8).

By this procedure, we obtained a set of oxygen binding constants which describe the available set of data with a good agreement (r^2 > 0.991 for all) and also are consistent between the different experimental conditions. For pH 7.5 and pH 7.8, the fitting of the Nested-MWC-model did not lead to well defined values of the allosteric equilibrium constants for the embedded samples. Thus, the conformational distribution should be taken with care. For pH 7.8 a more elaborate approach was applied to estimate the conformational distribution, since here additionally structural data are available.

	Deoxy^{EM}	Solution	Oxy^{EM}
pH 6.5		log Lt $\geq$ 16 log Lr $\geq$ 14 log (Λ*Lt²/Lr²) = 3.43 $\pm$ 0.03 $^{\$}$	
pH 7.5	log Lt = 9.1$\pm$0.2 2.1$\geq$log Lr $\geq$6.9$^{\$\$}$ log (Λ* Lt²/Lr²) = 1.85	log Lt = 7.70 $\pm$ 0.07 log Lr = 2.1 $\pm$ 0.4 log Λ = -9.5 $\pm$ 0.8	
pH 7.8	log Lt $\geq$ 9 log Lr = 2.47 $\pm$ 0.09 log Λ = -12.74 $\pm$ 0.37	log Lt = 6.1 $\pm$ 0.2 log Lr =1.85 $\pm$ 0.08 log Λ = -8.3 $\pm$ 0.1	log Lt = 6 $\pm$ 3 (log Lt $\leq$5) log Lr = 1.1 $\pm$ 0.1 (log Lr = 1.05) log Λ= -9.9$\pm$ 0.9 (log L = -9.16)
pH 6.5 + L		log Lt undefined log Lr = 2.97 $\pm$ 0.07 log Λ $\leq$ -35	
pH 7.8 + L		log Lt $\leq$ 2 log Lr $\leq$ -1 log Λ = -4.99 $\pm$ 0.09	

Tab. S7. Allosteric equilibrium constants and conformational distributions: Setting the oxygen binding constants fixed to the values summarized in Tab. S6 each set of data was analyzed individually to obtain the corresponding allosteric equilibrium constants. In those cases where some of the allosteric equilibrium constants tend to develop to very high or low values, indicating that particular conformations are completely suppressed, the range of values yielding the same sum of squared residuals as the free-running fit were determined. In some cases only two of the three allosteric equilibrium constants are defined, the third being dependent on the other two. In case of pH 7.8 Oxy^{EM}, an alternative set of values was determined based on additional information from structural data (*see below*), yielding the allosteric equilibrium constants given in parenthesis.

$$\Lambda = L\frac{(1+l_R)^2}{(1+l_T)^2} = \frac{[rT,rT]_o}{[rR,rR]_o}$$

$^{\$}$ data define only the product of allosteric equilibrium constants as given.

$^{\$\$}$Determined manually, criterium: $SS^2 < SS^2_{min}$ (SS^2= sum of squared residuals); here, L is no independent parameter, but has to fulfill the equation given above

	Deoxy^{EM}		**Solution**		**Oxy^{EM}**	
	0 Torr	760 torr	0 Torr	760 torr	0 Torr	760 torr
pH 6.5	x_{tT}=0.90±0.08 x_{tR}=0.1±0.1		$x_{tT,0}$ =1	$x_{tR,760}$ = 1	x_{tR}=0.91±0.08	
pH 6.5 + L	x_{tR} = 0.6 ± 0.2 x_{rR} = 0.4 ± 0.2		$x_{tR,0}$ = 1	$x_{rR,760}$ = 0.98	x_{tR} = 0.3 ± 0.2 x_{rR} = 0.6 ± 0.2 x_{rT} = 0.13 ± 0.07	
pH 7.8 + L	x_{rR} = 1.0 ± 0.1		$x_{rR,0}$ = 0.83	$x_{rT,760}$ = 1	x_{rT} = 0.97 ± 0.05	
pH 7.5	$x_{tT,0}$ = 0.99 *	$x_{rT,760}$ = 0.91*	$x_{tT,0}$ = 0.98	$x_{rT,760}$ = 0.99	x_{rR} = 0.9 ± 0.2	
pH 7.8	$x_{tT,0}$ = 0.68* $x_{tR,0}$ = 0.32*	$x_{tR,760}$ = 0.10* $x_{rR,760}$ = 0.90*	$x_{tT,0}$ = 0.66 $x_{tR,0}$ = 0.34	$x_{rT,760}$ = 0.96	$x_{tR,0}$ = 0.86 *	$x_{rR,760}$ = 0.65* $x_{rT,760}$ = 0.35*
pH 7.8 adjusted					$x_{tR,0}$ = 0.92	$x_{rR,760}$ = 0.25 $x_{rT,760}$ = 0.75

Tab. S8. Conformational distributions: Based on the parameters shown in Tab. S6 and S7, the conformations were calculated for 0 and 760 Torr, respectively, in case of cooperative binding curves (*denoted by x with the corresponding suffix*). For those cases where the entrapment in the sol-gel arrested the conformations, the corresponding distribution was determined based on fitting a sum of hyperbolic curves to the data according to eq.6 (grey shaded cells). Since here the distribution is the same for all oxygen concentrations, no additional suffix is given. The asterisks indicate the cases where the allosteric equilibrium constants are not well defined and therefore the calculated conformational distribution is not well based. The robustness of the conformational distribution was addressed for pH 7.5 and pH 7.8 *(see below*).

Stability of conformational distributions at pH 7.5 and pH 7.8 in absence of L-lactate

The following strategy was applied: first, within the range defined by the error in the allosteric equilibrium constants as provided by the fitting routine, a set of 10 values was calculated for each of the allosteric equilibrium constants (equidistant on the logarithmic scale). For each of the possible combinations of allosteric equilibrium constants, the conformational distribution at 0 Torr and 760 Torr and the sum of squared residuals was calculated. From these, only the range (SS^2_{min}, $2*SS^2_{min}$) was considered, to remain reasonable close to the data.

For solution data at pH 7.5, the deviation of those parameter values complying with this range of SS^2min-values from the values given in Tab. S8 were less than 10% (absolute value), thus in solution under fully saturated conditions conformation rT seems to prevail while under deoxygenated conditions it is conformation tT. For $Deoxy^{EM}$ the distribution in absence of oxygen remains to be strongly dominated by tT, in agreement with solution data. At 760 Torr a possible scenario with about 55% rR and 45% rT could be identified with a 50% increase in SS^2, compared to 91% rT for lower values of SS^2. The parameter values for hemocyanin in the Oxy^{EM}-state are well defined, thus the comparison with the solution data indicates that there is some tendency of the sol-gel to stabilize rR compared to rT, yielding to a dominant population of rR at 760 Torr for Oxy^{EM} and possible also some fraction for $Deoxy^{EM}$.

For data at pH 7.8, the corresponding patterns of conformational distributions are summarized in Fig. S7. The stability test reveals that the oxygenated conformation (panel B) for solution data (rT, black) and $Deoxy^{EM}$ (rR, red) are well defined. In contrast, under deoxygenated conditions, conformation tT could range between 0.4 and 1.0 for both conditions (Panel B, black and grey) and the distribution is in agreement with the expectation that for these two conditions the conformational distribution should be similar. The conformational distribution for Oxy^{EM} is much more variable thus it is less well defined than the other two both under oxygenated and deoxygenated conditions. Thus, to find out whether a conformational distribution with a high amount of rT under oxygenated conditions (similar to solution data in panel B) and a low amount of tT under deoxygenated conditions (unlike $Deoxy^{EM}$ and solution data in panel A) is compatible with the data, the values highlighted by the grey box in panel B (maximal values for rT_{760}) were selected, and among those the one with tT_0<0.3 (red box in panel A). All these values have in common a value of log Λ= - 9.156. Thus, the binding data for Oxy^{EM} were re-analyzed setting this allosteric equilibrium constant fixed. The analysis yielded log Lt ≤ 5 and log Lr = 1.06 ± 0.12 (Tab. 7S) with $SS^2=1.5*SS^2_{min}$.

These results indicate that a dominant population of rT under oxygenated conditions for Oxy^{EM} is in agreement with the binding data, and thus agree with the structural data.

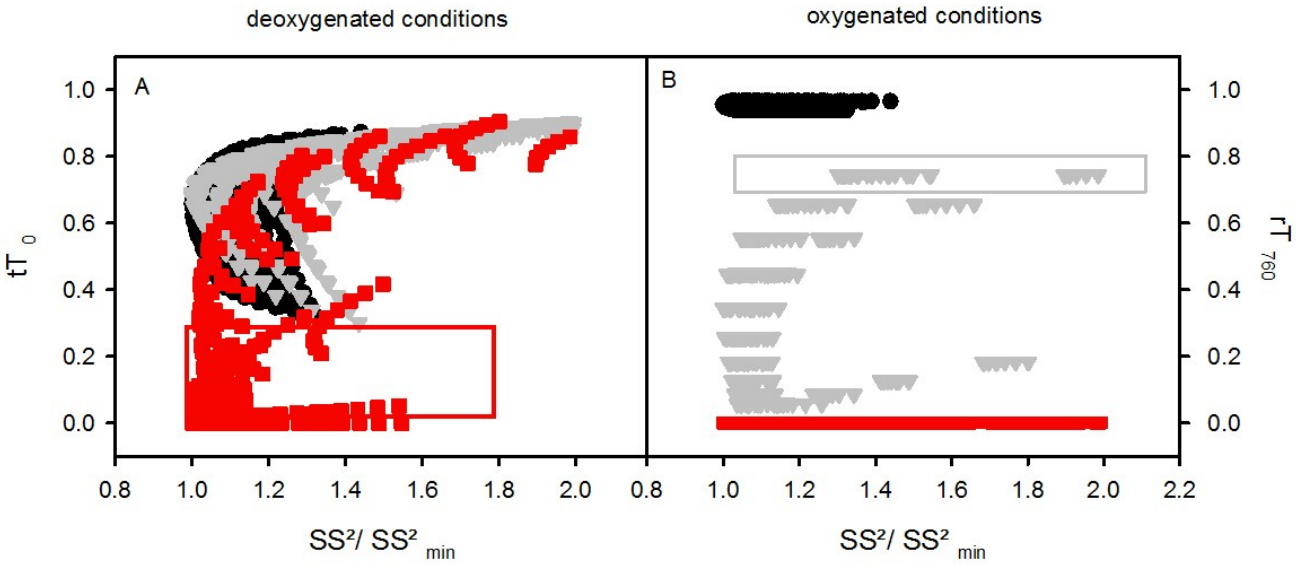

Fig. S7: Analysis of the conformational distribution at pH 7.8: The calculated values for conformation tT in absence of oxygen (tT_o, *panel A*) and for rT at 760 torr (rT_{760}, *panel B*) were calculated for different combinations of allosteric equilibrium constants yielding binding curves which agree with the data to an extent defined by $SS^2<2*SS^2_{min}$. In all relevant cases for the deoxygenated state only the two conformations tT and tR had to be taken into account, while for oxygenated conditions only rR or rT occurred. For each panel, the situation which should differ from the other two based on structural data (see Fig. 6) is depicted in red squares. Panel A: solution data (*black circles*) and $Deoxy^{EM}$ (*grey triangles*) should agree, whereas Oxy^{EM} (*red squares*) should differ. Panel B: solution data (*black circles*) and Oxy^{EM} (*grey triangles*) should agree, whereas $Deoxy_{EM}$ (*red squares*) should differ.. The grey box indicates the range selected for $Oxy_{760}{}^{EM}$ based on this ranking, the red box the values selected for $Oxy_0{}^{EM}$ (*see text for details*).

References in Supplementary Information

64. G. Lelong, D. L. Price, J. W. Brady and M. L. Saboungi, *J. Chem. Phys.,* 2007, **127**, 065102, DOI: 10.1063/1.2753841

65. E.M. Rabinovich, *The Springer International Series in Engineering and Computer Science,* 1994, **254**, 1-37.

66. B. N. Nair, W. J. Elferink, K. Keizer and H. Verweij, *J. Coll. Interf. Sci.,* 1996, **178**, 565-570.

67. P.A. Srere, G. W. Kosicki and R. Lumry, *Biochim. Biophys. Acta,* 1961 ***50****, 184-185.*